Deformation of stem cell nuclei by nanotopographical cues†

Kevin J. Chalut,‡[ab] Karina Kulangara,‡[b] Michael G. Giacomelli,[b] Adam Wax[b] and Kam W. Leong*[bc]

Received 23rd October 2009, Accepted 14th January 2010
First published as an Advance Article on the web 19th February 2010
DOI: 10.1039/b921206j

Cells sense cues in their surrounding microenvironment. These cues are converted into intracellular signals and transduced to the nucleus in order for the cell to respond and adapt its function. Within the nucleus, structural changes occur that ultimately lead to changes in the gene expression. In this study, we explore the structural changes of the nucleus of human mesenchymal stem cells as an effect of topographical cues. We use a controlled nanotopography to drive shape changes to the cell nucleus, and measure the changes with both fluorescence microscopy and a novel light scattering technique. The nucleus changes shape dramatically in response to the nanotopography, and in a manner dependent on the mechanical properties of the substrate. The kinetics of the nuclear deformation follows an unexpected trajectory. As opposed to a gradual shape change in response to the topography, once the cytoskeleton attains an aligned and elongation morphology on the time scale of several hours, the nucleus changes shape rapidly and intensely.

1. Introduction

Nuclear architecture and organization influence cell function.[1] The nucleus is exposed to forces generated within the cell and forces transmitted through the cytoskeleton from outside the cell.[2] Thus the nucleus acts as a mechanosensor.[3] Insights on the mechanisms by which environmental forces are transmitted to the nucleus are emerging: the nucleus is coupled to the cytoskeleton *via* the inner nuclear membrane proteins SUN1 and SUN2;[4–7] nesprin proteins bind to SUN proteins *via* their conserved C-terminal KASH domain (Klarsicht, Anc-1, Syne homology);[8] nesprin-3 binds to plectin, which associates with intermediate filaments;[9] and the larger isoforms nesprin-1 and nesprin-2 bind to actin.[6] By this pathway, forces are relayed from the extracellular matrix *via* the cytoskeleton to the nucleus. These forces, along with internally generated forces, can lead to changes in nuclear shape, leading to conformational adaptation in chromatin structure and organization, which in turn affects transcriptional regulation.[10]

There are many types of external cues that can alter the morphology of the cell body and nucleus, including changes in pH, temperature, extracellular osmolarity, oxygen tension, and mechanical stiffness of the substrate. Topography emerges as another cue being increasingly investigated for manipulation of cell function. Nanotopography, which has been incorporated into both 2-D and 3-D constructs, can mimic some of the features of extracellular matrix and affect proliferation and differentiation in cell culture.[11–14] The underlying molecular mechanisms remain elusive. We hypothesize that the nanotopographical cues are transmitted directly from focal contacts to the nucleus, where nuclear reorganization can alter cell function. As an attempt to better understand these nanotopography-mediated phenomena, this paper focuses on studying the kinetics of nuclear shape change by a non-invasive optical technique.

Although many studies have explored the changes of cell shape in response to environmental stimuli, few have explored the structural changes of the cell nucleus. Two factors render such study difficult. First, the refractive index of the nucleus differs from that of the cytoplasm by less than 4%,[15] so there is not a high level of contrast available for light microscopy. Second, although fluorescence microscopy can be used to image the stained nucleus, the technique is invasive and not easily amenable to population analysis. The labor-intensive procedure of fixing, imaging, and manually analyzing a large number of cells also prohibits detailed kinetic analysis.

One technique that can overcome the limitations listed above is inverse light scattering analysis (ILSA). ILSA deduces structure and organization in a sample[16] in three steps:[17] the measurement of the far-field diffraction pattern of a sample, which is a unique signature of the size, shape, organization, and electromagnetic properties of a sample;[18,19] appropriate processing to isolate the scattering contribution from the structure of interest in a sample when necessary;[17] and the correlation of the processed signal with a theoretical light scattering model to deduce the most probable scattering configuration.[20] In the present study, the light scattering profile from an ensemble of hMSCs on nanogratings (350 nm width, 350 nm height, and 700 nm pitch) is measured, and then processed to isolate the contributions from the cell nucleus, followed by matching the data with light scattering profiles calculated by a T-matrix model.[21] This T-matrix model predicts the light scattering profiles from spheroid-shaped objects such as cell nuclei.[22] From the ILSA algorithm we developed,[21] we are able to deduce the average size and aspect ratio of hundreds of cell nuclei within minutes.

The light scattering technique used for this study is angle-resolved low coherence interferometry (a/LCI), which uses low

[a]*Department of Physics, University of Cambridge, Cambridge, CB3 0HE, UK*
[b]*Department of Biomedical Engineering, Fitzpatrick Institute for Photonics, Duke University, Durham, NC, 27708, USA*
[c]*Department of Surgery, Duke University, Durham, NC, 27710, USA*
† Electronic supplementary information (ESI) available: Supplemental movies 1–2. See DOI: 10.1039/b921206j
‡ These authors contributed equally to this work.

coherence light to achieve optical sectioning for rejecting light scattered multiple times that contributes noise to the scattering distribution.[17] Additionally, the a/LCI technique detects back-scattered light, which is sensitive to scattering from cell nuclei[23] from a biological sample. Recently, a/LCI has been successfully applied to assessing nuclear shape[24] and assessing subcellular organization in cell culture.[25] The use of a T-matrix light scattering model for the ILSA algorithm is a recent inclusion in the a/LCI technique to provide additional information about nuclear morphology and subcellular organization. This study illustrates the appeal of a/LCI in tracking the kinetics of nuclear deformation. It reveals the interesting response of hMSC to nanopatterns over a period of two days of culture. The nuclei elongate more rapidly on the more rigid polystyrene nanogratings than on the PDMS counterpart. The nuclear deformation is also nonlinear with time.

2. Experimental

2.1 Soft lithography

The nanopattern master mold was produced by nanoimprinting as previously described.[11] The nanopattern was reproduced on poly(dimethylsiloxan) (PDMS) (Sylgard 184 Silicone Elastomer Kit; Dow Corning, Midland, MI) using soft lithography on the nanoimprinted poly(methyl methacrylate) (PMMA)-coated Si master mold. The gratings on the nanoimprinted PMMA master molds were 350 nm in depth, 350 nm in width, and 700 nm in pitch. The PDMS replicas were fabricated with an elastomer base/cross-linking agent ratio (w/w) of 10 : 1, Young's modulus 400kPa, degassed, poured onto the PMMA-coated Si master mold, allowed to bake at 50 °C for 3 h, cooled at room temperature, and then separated from the mold. Patterned PDMS samples were either used directly for the imaging experiments or used as a mold for nanoimprint lithography (Scheme 1).

2.2 Nanoimprint lithography

Glass coverslips no.1.5 (VWR, West Chester, PA) were spin-coated with 10% polystyrene (Sigma- Aldrich, St. Louis, MO) in toluene (w/v) (Sigma-Aldrich, St. Louis, MO) at a ramp speed of 300 rpm for 10 s and a speed of 3000 rpm for 40 s to form a 500 nm thick film. After solvent evaporation for 5 days the polystyrene-coated coverslips were heated to 220 °C for 1 min. A pressure of 50 kPa was used to emboss the PDMS mold into the molten PS film. After 45 s ice water was used to cool down the system and the film was peeled off the PDMS mold when the temperature was below 30 °C. The coverslips with the planar or nanograted polystyrene films with a Young's modulus of 3GPa were glued into a 2-well glassbottom chamber (Labtek, VWR, West Chester, PA) using a UV curable glue (Loctite, Henkel, Germany) under UV exposure for 15 min. For cell culture the polystyrene and PDMS substrates were coated with collagen I (BD Biosciences, Bedford, MA) at 15 μg/cm^2 to reduce the surface hydrophobicity (Scheme 1).

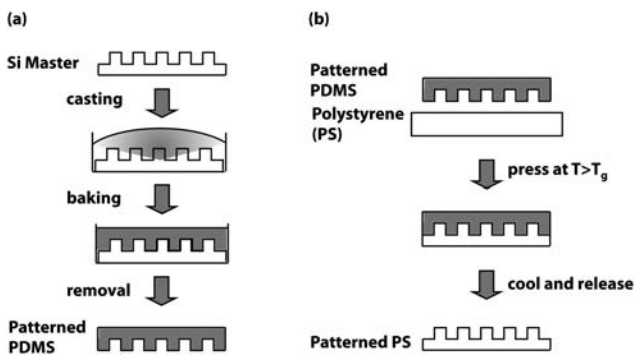

Scheme 1 Fabrication of nanogratings. (a) PDMS nanogratings are fabricated using soft lithography. PDMS mixed with its crosslinker is casted onto the Si master. After baking the patterned PDMS is separated from the Si master. (b) PS nanogratings are fabricated using nanoimprinting. A PDMS mold is used to emboss nanogratings into the viscous PS at a temperature above the Tg of PS. After cooling the patterned PS is separated from the PDMS mold.

2.3 hMSC cell culture

Human mesenchymal stem cells P1 were obtained from Dr Prockop's laboratory at Tulane University. hMSCs were cultured in α-minimal essential medium (Invitrogen/Gibco, Carlsbad, CA) containing 20% (v/v) fetal calf serum (Atlanta Biologicals, Lawrenceville, GA), 2 mM glutamine (Invitrogen/Gibco, Carlsbad, CA), 1% penicillin streptomycin (Invitrogen/Gibco, Carlsbad, CA). P3 hMSCs were plated onto collagen I-coated polystyrene films or PDMS surfaces at a density of 6000 cells per cm^2.

2.4 Immunostaining

hMSCs were fixed at different time points in 4% paraformaldehyde for 12 min and the nuclei were stained with 4′,6-diamidino-2-phenylindole (DAPI) (Invitrogen/Molecular Probes), and F-actin was stained with Alexxa488 conjugated phalloidin (Invitrogen/Molecular Probes) in the presence of 0.3% Triton X-100 for 30 min. hMSCs were washed twice in PBS and mounted (Biomeda, Foster City, CA). Confocal images were taken on a Zeiss 510 inverted confocal microscope using a 40× objective.

2.5 Quantitative image analysis (QIA)

The long and short axis of each stained nucleus was measured using the Zeiss imaging software. Their aspect ratio was obtained by dividing the short over the long axis. Alignment was defined by the degree to which the long axis of an elongated nucleus was oriented with respect to the grating. Nuclei were considered aligned if the angle between the long axis and the grating was $< 15°$. The percentage of nuclear alignment and ratio of the short and long axis was measured. For all indicated timepoints, the statistics for at least 50 nuclei was compiled.

2.6 a/LCI measurements

Kinetics studies were performed on hMSC nuclei over two different time courses, 12 h and 48 h. The 12 h study was designed to take a closer look at the early kinetics of the nucleus. For the 48 h kinetics study, at least 4 samples for each condition (cultured on ngPS or ngPDMS) were prepared; for the 12 h study 8 ngPS samples were prepared. Each measurement time point was

acquired at room temperature in less than 15 min. Following the a/LCI experiments, the samples were fixed and stained for DAPI and subjected to confocal microscopy and subsequent image analysis. In the 48 h kinetics study, each data point represents 10–12 a/LCI measurements, while in the 12-hour kinetics study, each time point represents 23–25 measurements. Each a/LCI measurement included scattering information from ~50 cell nuclei, and the duration of each measurement was approximately 3 min. Therefore, up to 1000 cells were interrogated every hour using the a/LCI technique. The results of the ILSA algorithm (see following section) for each measurement would be compiled and statistically analyzed. Final results were recorded as mean ± SD unless otherwise noted, and statistical significance was determined using a ranksum test. For information about the optical setup of a/LCI, see ref. 17.

2.7 Statistics of ILSA algorithm

After the scattered light from a distribution of cells was measured, the data were input into the ILSA algorithm. The ILSA algorithm involves the processing of the light scattering signal and comparison to a database of appropriately parameterized theoretical light scattering signals. The light scattering signals are modeled using a T-matrix based analysis.[26] For detailed information about the implementation of the T-matrix based ILSA algorithm, see ref. 21 and the online supplement to ref. 25. For the present study, the cutoff frequency used for processing the measured light scattering signal by low-pass filter corresponded to a size scale of 18 microns. The purpose of the low pass filtering step is to remove the contribution of frequencies corresponding to whole-cell scattering and higher order correlations of subcellular scattering from the light scattering signal. The resulting processed signal contains contributions from the nucleus and scattering objects smaller than the nucleus. The ILSA algorithm compares the processed nuclear scattering data to a database of scattering distributions predicted by T-matrix modeling using a least-squares ($\chi 2$) fitting routine. The database prepared for the ILSA algorithm was parameterized in the following way: equal volume diameter (EVD, defined as the diameter of a sphere with the same volume as the spheroid) between 12.0 and 18.0 microns in increments of 0.1; aspect ratio (ε) between 0.5 and 0.85 in increments of 0.01; index of refraction of cytoplasm of 1.35 and 1.36; index of refraction of nucleus of 1.41 and 1.42; and normally distributed EVDs with 5.0% and 10.0% standard deviation about the center EVD. These ranges of values were chosen based upon quantitative image analysis (QIA) of typical hMSC nuclei. The refractive index combinations were determined by an ILSA algorithm that held EVD and ε constant (14.5 μm and 0.7, respectively, determined by QIA) while spanning a wide range of refractive index combinations (1.33–1.38 for cytoplasmic index of refraction and 1.39–1.46 for nuclear index of refraction). EVD and ε are the final output of the ILSA algorithm for an individual measurement.

2.8 Transfection

hMSCs were transfected with 4 μg of GFP-lifeact[27] using lipofectamine 2000 (Invitrogen), according to the manufacturer's protocol.

2.9 Live cell imaging

GFP-actin positive hMSCs were trypsinized and plated onto glass coverslips spincoated with polystyrene and subsequently nanoimprinted as previously described. Seeded cells were imaged using an inverted live cell imaging system (Zeiss Axiovert Observer) with a 40× oil objective. Images were acquired every 2.5 min using Metamorph software.

3. Results

For QIA, the long and short axis of the hMSC nuclei and their alignment along the grating axis were measured using the Zeiss imaging software and their aspect ratio ε calculated (Fig. 1). hMSC nuclei were 56% aligned at 6 h and 73% aligned at 48 h after plating on PDMS nanogratings (ngPDMS). On the polystyrene nanogratings (ngPS), however, the alignment was more pronounced: 77% at 6 h and 80% at 8 h and beyond. There was a dramatic increase of alignment of the nuclei between 4 h and 6 h on ngPS, from 42% to 77%. On both the PDMS and the PS surfaces, nuclear elongation over time paralleled the cell alignment to the gratings. There was no discernible change in the projected area of the nuclei throughout the study on either ngPDMS or ngPS.

For all controls (planar PDMS and planar PS at $t = 0$ h and $t = 48$ h) and initial measurements of ngPDMS and ngPS, the aspect ratio measured by both QIA and a/LCI was between 0.69 and 0.71 with a SD between 0.08 and 0.12. According to QIA, the nuclear elongation on both ngPDMS and ngPS became statistically significant ($p < 0.05$) at $t = 6$ h and remained so for all later time points. The a/LCI measurements of both ngPDMS and ngPS agreed, within error, with the QIA measurements at all time points (see Fig. 2). At all times, the EVD remained relatively consistent, ranging between 12.5 and 15.0 μm and with a SD between 10% and 20% for both QIA and a/LCI.

Dramatic changes in the aspect ratio, ε, were observed using the a/LCI technique, with 15% changes in aspect ratio observed within 12 h, and over 20% by the second day of observation. These changes in ε corresponded to an elongation of the nucleus along the direction of the nanograting. At $t = 3$ h on ngPS, the nuclei began to orient, and elongated to $\varepsilon = 0.65 \pm 0.09$ (mean ± SD), and by $t = 6$ h and $t = 12$ h, the nuclei had reached $\varepsilon = 0.62 \pm 0.09$ and $\varepsilon = 0.60 \pm 0.07$, respectively. At $t = 24$ h on ngPS, the nucleus was elongated to $\varepsilon = 0.55 \pm 0.03$. No further elongation on ngPS was observed using the a/LCI technique beyond $t = 24$ h. It should be noted that $\varepsilon < 0.5$ is not accessible by T-matrix calculation and therefore the ILSA algorithm was not parameterized below $\varepsilon = 0.5$. Given a ~10% SD, the floor imposed by limits of the T-matrix calculation is likely to skew the results of the aspect ratio upwards as the nuclei achieve aspect ratios at or below $\varepsilon = 0.5$. All a/LCI results for ngPS demonstrated a statistically significant ($p < 0.05$) difference from all controls at $t = 6$ h and beyond. Additionally, at all time points the a/LCI results are very similar to the results of QIA, which has no floor on the measurement of aspect ratio.

In the 48 h a/LCI kinetics study of hMSCs on ngPDMS, nuclear elongation along the direction of the grating was also observed, but not to the extent of the elongation observed on ngPS. The nuclei became elongated on ngPDMS through $t = 3$ h

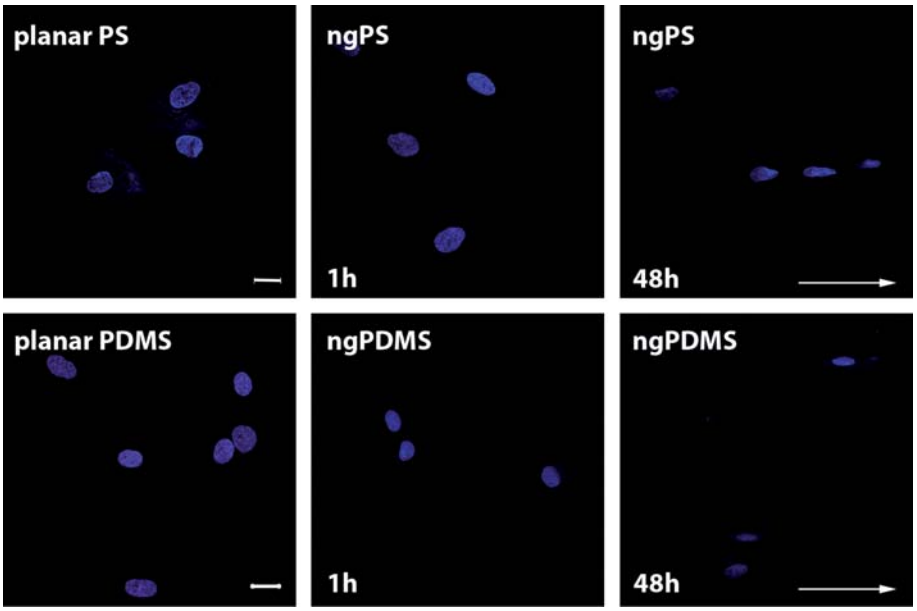

Fig. 1 Fluorescence micrographs of DAPI-stained human mesenchymal stem cell nuclei. The two leftmost panels indicate the nuclei on planar polystyrene (PS) and planar PDMS substrates. The two middle panels show the nuclei on the nanograted substrates (ngPS and ngPDMS) after $t = 1$ h. The two right most panels show the nuclei on ngPS and ngPDMS after $t = 48$ h. Notice that the nuclei orient and extend along the axis of the grating at $t = 48$h. The grating axis is indicated by the arrow. Scale bar 15 μm.

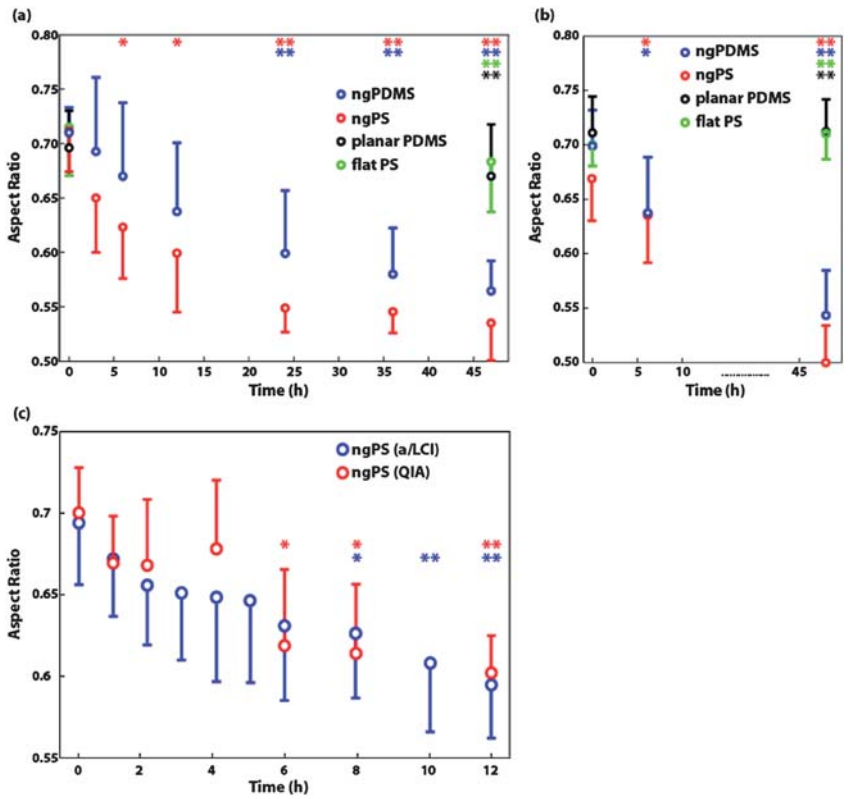

Fig. 2 (a) a/LCI results of the average shape change of the hMSC nucleus over 48 h. Error bars represent SEM within 95% confidence interval. Red and blue asterisks indicate statistical significance of the difference in shape for ngPS and ngPDMS, respectively, between the time point and the nucleus shape measurement on planar control at $t = 0$ h (* indicates $p < 0.05$ and ** indicates $p < 0.01$ as calculated from a ranksum test). (b) QIA results following same color convention as (a). (c) a/LCI and QIA results of the average shape change of the hMSC nucleus over 12 h. Blue and red asterisks indicate statistical significance of the difference in shape using a/LCI and QIA, respectively, between the time point and the nucleus shape measurement on ngPS at $t = 0$ h.

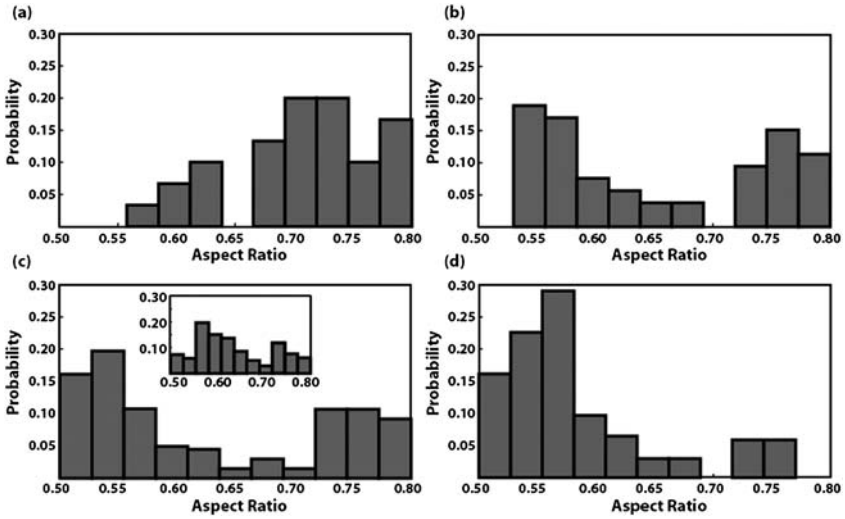

Fig. 3 Histograms of the aspect ratio of the hMSC nuclei as measured by a/LCI at (a) 1 h, (b) 3 h, (c) 6 h, and (d) 12 h. $N = 40$ for all time points. Inset: QIA measurements of the hMSC nuclei at 6 h ($N = 40$). Notice the bimodal distribution of shapes at 3 h and 6 h.

($\varepsilon = 0.69 \pm 0.10$), $t = 6$ h ($\varepsilon = 0.67 \pm 0.10$), and $t = 12$ h ($\varepsilon = 0.64 \pm 0.09$). The difference between the aspect ratios at $t = 24$ h ($\varepsilon = 0.60 \pm 0.09$) and all controls became statistically significant ($p < 0.05$), and remained so at $t = 36$ h ($\varepsilon = 0.58 \pm 0.04$) and $t = 48$ h ($\varepsilon = 0.56 \pm 0.05$).

The 12 h a/LCI kinetics study was performed to look at a larger sample size on ngPS during early time points. In this study, the results indicated a significant elongation between $t = 0$ and $t = 12$ h (Fig. 2c). The results at $t = 3$ h, $t = 6$ h, and $t = 12$ h were very similar to the results in the 48 h a/LCI kinetics study. Significant differences ($p < 0.05$) from the aspect ratio at $t = 0$ h were observed at $t = 8$ h ($\varepsilon = 0.63 \pm 0.09$), and highly significant differences ($p < 0.01$) from the aspect ratio at $t = 0$ h were observed at $t = 10$ h ($\varepsilon = 0.61 \pm 0.09$) and $t = 12$ h ($\varepsilon = 0.59 \pm 0.07$). An interesting observation resulting from these measurements, and the measurements of QIA, was that very little change occurred in nuclear elongation between $t = 2$ h ($\varepsilon = 0.66 \pm 0.09$) and $t = 5$ h ($\varepsilon = 0.65 \pm 0.11$). All results from the 48 h and 12 h kinetics studies, for both QIA and a/LCI, are presented in Fig. 2. Additionally, the distribution of the aspect ratios of the nuclei as measured by a/LCI at $t = 1$ (after attachment), 3, 6, and 12 h is presented in Fig. 3. The distribution of aspect ratios is distinctly bimodal at $t = 3$ and 6 h, for both a/LCI and QIA measurements.

3.1 Live cell imaging

According to Fig. 2c, the nuclei underwent a fairly rapid deformation between 0 and 2 h. Timelapse video microscopy showed that during this time cell adhesion to the substrates took place (see supplemental movie 1†). Furthermore, we observed in both a/LCI and QIA results that there was ostensibly little nuclear deformation in hMSCs occurring between 2 and 5 h on the ngPS substrate. We hypothesized that, during the initial 5 h, hMSCs sensed the environment and a rearrangement of the cytoskeleton took place. To test this hypothesis, we transfected hMSCs with GFP-Lifeact, a 17-amino-acid peptide that stains filamentous actin structures without interfering with its dynamics.[27] Transfected cells were then plated on 350 nm grating PS dishes and imaged at 37 °C and 5% CO_2 using a live-cell imaging system (Zeiss Axio Observer). The images revealed that during the initial 2 h a flattening and spreading of the cells occurred. After 6 h and 8 h the F-actin fibers oriented in the direction of the nanogratings and nuclear deformation became more pronounced (Fig. 4a, supplemental movie 2†). Aligned and elongated F-actin fibers of cells fixed after 48 h on ngPDMS were visualized by Alexxa 488 labelled phalloidin (Fig. 4b).

4. Discussion

A promising application of continuous nanostructures is their use as a biomimetic substrate to modulate certain cell functions. Such nanostructures can mimic the topography of the extracellular matrix. Several reports demonstrate that nanoscale features in a culture environment can alter the morphology of cell body and cell nucleus and induce differentiation in stem cells, including hMSCs and embryonic stem cells.[12,14,28] Nanoscale features initiate signals from the cell-matrix adhesions that are transduced to the nucleus through the cytoskeletal network, from actin stress fibers to the intermediate filament network of the nucleus. We have previously shown that the nanogratings dictate cell adhesion and alter the adhesion structure.[29] Moreover, we previously analyzed the alignment of the actin cytoskeleton along the nanogratings.[14] On nanogratings hMSCs form small focal complexes associated with motility, as opposed to larger focal adhesions associated with increased formation of stress fibers (unpublished results), cell spreading, and an increase in metabolic activity and proliferation.[30]

The intermediate filament network forms a direct, solid-state connection through which signals are transmitted from the cell periphery to the cell nucleus.[31,32] The nuclear envelope comprises a stiff lamin network[33] through which the more viscous chromatins can move and into which chromatins can bind. Chromatins are charged and they are mechanically integrated with the cytoskeleton through the lamin network, hence they are extremely sensitive to the osmotic environment[34] as well as forces

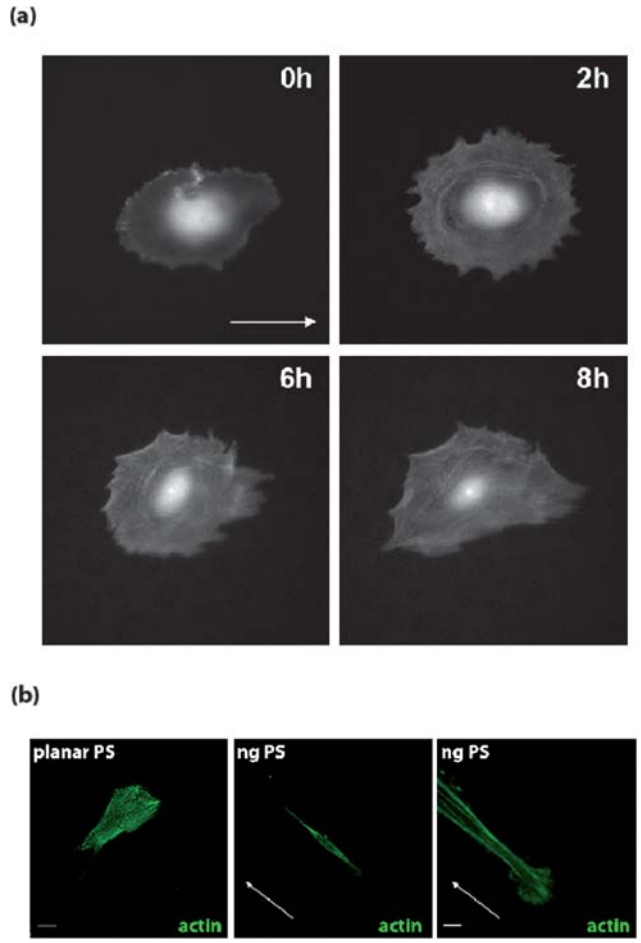

Fig. 4 Actin cytoskeleton rearrangement before nuclear deformation. (a) hMSCs transfected with GFP-lifeact plated on ngPS substrates. Images were taken at 2 h, 6 h and 8 h after plating. Between 0 h and 2 h a flattening and spreading of the hMSCs occurred, with the actin filament rearranging in response to the topography. Spreading on the substrate was visible at 6 h and 8 h after plating. (b) hMSCs were fixed and F-actin was stained with phalloidin 48 h after plating. The F-actin filament ran parallel to the grating direction as indicated by a white arrow. Scale bar left most panel 20 μm, right most panel 5 μm.

transduced from the environment.[35] Therefore, reorganization of the lamin network brought about by external cues propagated through the cellular network alters the chromatin accessibility to transcription factors and hence gene expression. These changes lead to changes in proliferation, differentiation or cell death. Although the mechanisms by which topographical cues influence cell-matrix adhesions and the downstream signaling pathways are beginning to be elucidated, many questions remain.

In the present study we demonstrate how the cell nuclei respond to nanogratings, which alters gene expression and hence cellular function.[36] Using quantitative image analysis and light scattering techniques (a/LCI), we gain insights into the kinetics of nuclear deformation in response to nanotopography. We report the elongation of human mesenchymal stem cell nuclei as a specific response to nanotopography. This response is dramatic over a period of 12 h, and between 12 and 24 h, the nuclei gradually elongate along the direction of the grating, appearing

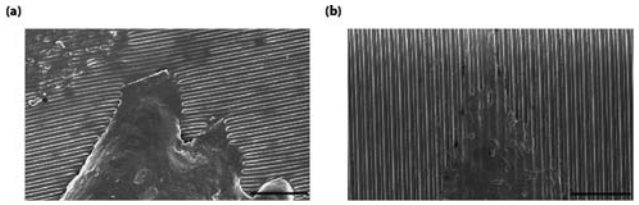

Fig. 5 SEM micrographs of hMSCs on nanograting substrates. (a) ngPDMS; the cell is able to deform the gratings at its extremities; (b) ngPS; no deformation is observed on this much stiffer substrate. Scale bar 5 μm.

to converge on an extension of approximately 2 : 1. This behavior is observed in both a/LCI and QIA. The time lapse video microscopy reveals that the initial rapid change in aspect ratio corresponds to the cell adhesion onto the nanogratings and the flattening of the cell.

An important result in the present work is the differing response of the hMSC nucleus to PDMS and PS nanogratings. We have previously observed that hMSCs can deform softer (Young's modulus $\sim$ 400 kPa) PDMS gratings (Fig. 5), hence intracellular forces may not be as prominent as they are on the stiff (Young's modulus $\sim$ 3 GPa) PS surface.[37] Intuitively, the mechanical activity of a cell is more efficient on a stiffer substrate, which is commensurate with the formation of focal adhesions and stress fibers.[38] Increased formation of stress fibers in the actin cytoskeleton would result in additional strain within the intermediate filament network, thereby increasing the mechanical forces on the nucleus.

A third noteworthy result involves the observation of the bimodal shape distribution (Fig. 3) of the hMSC nuclei for the first six hours of observation. One might expect the response pattern to follow the relatively continuous trajectory of cellular adhesion, cytoskeleton orientation, cellular and cytoskeletal extension, followed by an elongation of the cell nucleus. However, this is apparently not the case. In both a/LCI and QIA, we observe a clear bimodal distribution of nuclear shape, either

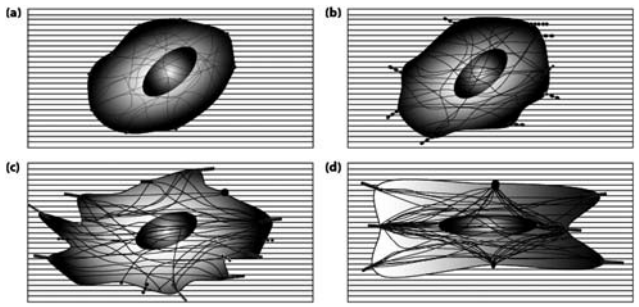

Scheme 2 The kinetics of nuclear elongation on nanogratings. The cell initiates attachment by sensing its environment, forming focal complexes, which become focal adhesions by applying force to their surroundings. Based on our results, we speculate that the force is most efficient in the direction of the grating. Focal adhesions would then elongate in this direction, and stress fibers would form preceding the alignment of the cytoskeleton. Forces within the stress fibers are propagated to the nucleus, which aligns with the cytoskeleton and elongates parallel to the grating.

round ($\varepsilon \sim 0.7$) or extended ($\varepsilon \sim 0.55$), with very few shape measurements in between.

We suggest two possibilities for the bimodal distribution and nonlinear kinetics of nuclear deformation, which indicates a complex relationship between adhesion, orientation, and nuclear elongation. First, the bimodally distributed aspect ratios between 2 and 6 h and the orientation results of QIA may reflect the distinctive uniaxial mobility of hMSCs on 350 nm gratings. During the course of 48 h the cells undergo several cycles of elongation in the grating direction followed by a release: the cells weakly attach, round up prior to a subsequent elongation, and then detach to form more rounded but weakly attached cells (supplemental movies†). The elongation-release behavior could explain the observation of a bimodal nuclear morphology. Another possibility is that the formation of cell-matrix adhesions, and cytoskeletal reorganization happens over a longer (~8–12 h) time scale, and then once the cytoskeleton is oriented in the direction of the nanogratings, the nuclear response occurs very rapidly (Scheme 2). This interpretation would explain why the nuclei seem to be either circular or elongated. According to Dahl *et al.*,[2] small nuclei are relaxed and large nuclei under tension; they show that the nuclear lamina forms a shell of interconnected rods that is extensible but limited in compressibility. It is tempting to speculate that hMSCs on nanogratings are exposed to tension parallel to the grating axis but experienced little tension in the perpendicular direction.

Finally, a/LCI represents a promising and novel way of observing the kinetics of the nucleus in response to extracellular cues. It is noteworthy that the ILSA algorithm employed by the a/LCI technique assumes spheroidal shaped nuclei; however, the hMSC nuclei possess an ellipsoidal shape. Nonetheless, the results of the a/LCI technique are in excellent agreement with the results of QIA, so it is apparently robust enough for small deviations from spheroidal shapes. This robustness was demonstrated and explored in other studies.[22,24] The a/LCI technique in its current form would not be effective for studying nuclei whose shape deviates greatly from a spheroid. Currently, the T-matrix model that serves as the foundation for the ILSA algorithm is limited to EVDs below 20.0 μm and aspect ratios above 0.5. With advances in computational power and powerful parallel processing techniques such as message passing interface (MPI), this restriction will be eased. Notwithstanding its current limitations, the a/LCI technique is a fast and efficient method for analyzing the kinetics of nuclear size and shape in most cell types.

5. Conclusions

In this study, we measured the response of the human mesenchymal stem cell nucleus to synthetic nanogratings. We observed significant extension of the stem cell nucleus along the axis of the grating over 2 days using two different techniques, a/LCI and fluorescence microscopy. The intensity of the response depended on the mechanical properties of the substrate. On the stiffer polystyrene substrate, the nuclei elongated more rapidly than on the softer PDMS substrate. Finally, the nuclei did not adhere to a gradual extension model; rather, they responded rapidly upon attachment, then exhibited a bimodal distribution of aspect ratios between 2 and 6 h, then gradually reached an extension of approximately 2 : 1 (axis parallel to grating to axis perpendicular to grating) between 6 and 48 h. The a/LCI technique offered robustness for this study. This non-invasive, high-throughput technique will be a valuable tool to correlate nuclear deformation with various forms of mechanotransduction in cellular studies.

Acknowledgements

This work has been supported by grants from the National Cancer Institute (R21CA120128-01, R33-CA109907), the National Institute of Health (HL 83008), the AOSpine Foundation, and the Swiss National Science Foundation (PBEL2-115950).

References

1 W. F. Marshall, *Mech. Dev.*, 2003, **120**, 1217–1230.
2 K. N. Dahl, *et al.*, *J. Cell Sci.*, 2004, **117**, 4779–4786.
3 J. Lammerding, *et al.*, *J. Clin. Invest.*, 2004, **113**, 370–378.
4 D. M. Hodzic, *et al.*, *J. Biol. Chem.*, 2004, **279**, 25805–25812.
5 V. C. Padmakumar, *et al.*, *J. Cell Sci.*, 2005, **118**, 3419–3430.
6 M. Crisp, *et al.*, *J. Cell Biol.*, 2006, **172**, 41–53.
7 F. Haque, *et al.*, *Mol. Cell. Biol.*, 2006, **26**, 3738–3751.
8 E. C. Schirmer, *et al.*, *Exp. Cell Res.*, 2007, **313**, 2167–2179.
9 K. Wilhelmsen, *et al.*, *J. Cell Sci.*, 2006, **119**, 5021–5029.
10 K. N. Dahl, *et al.*, *Circ. Res.*, 2008, **102**, 1307–1318.
11 E. K. Yim, *et al.*, *Biomaterials*, 2005, **26**, 5405–5413.
12 M. J. Dalby, *et al.*, *Nat. Mater.*, 2007, **6**, 997–1003.
13 K. T. Nguyen, *et al.*, *J. Nanosci. Nanotechnol.*, 2007, **7**, 2823–2832.
14 E. K. Yim, *et al.*, *Exp. Cell Res.*, 2007, **313**, 1820–1829.
15 J. R. Mourant, *et al.*, *Appl. Opt.*, 1998, **37**, 3586–3593.
16 Y. L. Kim, *et al.*, *IEEE J. Sel. Top. Quantum Electron.*, 2003, **9**, 243–256.
17 J. W. Pyhtila, *et al.*, *Opt. Express*, 2003, **11**, 3473–3484.
18 J. D. Wilson, *et al.*, *Biophys. J.*, 2005, **88**, 2929–2938.
19 H. K. Roy, *et al.*, *Gastroenterology*, 2004, **126**, 1071–1081; discussion 1948.
20 J. D. Wilson, *et al.*, *Opt. Lett.*, 2005, **30**, 2442–2444.
21 M. G. Giacomelli, *et al.*, *IEEE J. Sel. Top. Quantum Electron.*, 2009, DOI: 10.1109/JSTQE.2009.2031984.
22 M. G. Giacomelli, *et al.*, *Opt. Lett.*, 2008, **33**, 2452–2454.
23 A. Wax, *et al.*, *Biophys. J.*, 2002, **82**, 2256–2264.
24 K. J. Chalut, *et al.*, *Biophys. J.*, 2008, **94**, 4948–4956.
25 K. J. Chalut, *et al.*, *Cancer Res.*, 2009, **69**, 1199–1204.
26 M. I. Mishchenko, *et al.*, *Light Scattering by Nonspherical Particles: Theory, Measurements, and Applications*, Academic, 2000.
27 J. Riedl, *et al.*, *Nat. Methods*, 2008, **5**, 605–607.
28 S. Gerecht, *et al.*, *Biomaterials*, 2007, **28**, 4068–4077.
29 E. K. Yim, *et al.*, *Biomaterials*, 2009, **30**(6), 1133–1142.
30 M. J. Dalby, *et al.*, *Exp. Cell Res.*, 2004, **295**, 387–394.
31 A. J. Maniotis, *et al.*, *Proc. Natl. Acad. Sci. U. S. A.*, 1997, **94**, 849–854.
32 S. Hu, *et al.*, *Biochem. Biophys. Res. Commun.*, 2005, **329**, 423–428.
33 R. D. Goldman, *et al.*, *Genes Dev.*, 2002, **16**, 533–547.
34 F. Guilak, *J. Biomech.*, 1995, **28**, 1529–1541.
35 M. J. Dalby, *etal.*, *J. Cell. Biochem.*, 2007, **100**, 326–338.
36 C. H. Thomas, *et al.*, *Proc. Natl. Acad. Sci. U. S. A.*, 2002, **99**, 1972–1977.
37 U. S. Schwarz, *et al.*, *Med. Eng. Phys.*, 2005, **27**, 763–772.
38 I. B. Bischofs, *et al.*, *Proc. Natl. Acad. Sci. U. S. A.*, 2003, **100**, 9274–9279.